10-1-2016

Middle Permian U-Pb Zircon Ages of the "Glacial" Deposits of the Atkan Formation, Ayan-Yuryakh Anticlinorium, Magadan Province, NE Russia: Their Significance for Global Climatic Interpretations

V. I. Davydov
Boise State University

A. S. Biakov
Kazan Federal University

J. L. Isbell
University of Wisconsin-Milkwaukee

J. Crowley
Boise State University

M. D. Schmitz
Boise State University

Publication Information

Davydov, V.I.; Biakov, A.S.; Isbell, J.L.; Crowley, J.L.; Schmitz, M.D.; and Vedernikov, I.L. (2016). "Middle Permian U-Pb Zircon Ages of the "Glacial" Deposits of the Atkan Formation, Ayan-Yuryakh Anticlinorium, Magadan Province, NE Russia: Their Significance for Global Climatic Interpretations". *Gondwana Research, 38*, 74-85. http://dx.doi.org/10.1016/j.gr.2015.10.014

See next page for additional authors

Middle Permian U-Pb zircon ages of the "glacial" deposits of the Atkan Formation, Ayan-Yuryakh anticlinorium, Magadan province, NE Russia: Their significance for global climatic interpretations

Davydov, V. I.[1,2*](corresponding author), Biakov, A. S.[2,3], Isbell, J. L.[4], Crowley, J. [1], Schmitz, M. D.[1], and Vedernikov, I. L.[3]

[1]Department of Geosciences, Boise State University, Boise, ID, 83725, USA; (vdavydov@boisesate.edu, 1-208-4261119; JimCrowley@boisestate.edu; MarkSchmitz@boisestate.edu)
[2] Kazan Federal University, 18 Kremlyovskaya St., Kazan, Republic of Tatarstan 420008, Russia
[3] North-East Interdisciplinary Scientific Research Institute N.A. Shilo, Far East Branch of the Russian Academy of Sciences, 16 Portovaya St., Magadan 685000, Russia, abiakov@mail.ru; ivedernikov@rambler.ru)
[4] Department of Geosciences, University of Wisconsin–Milwaukee, Milwaukee, Wisconsin 53201, USA, jisbell@uwm.edu.

Abstract

The Atkan Formation in the Ayan-Yuryakh anticlinorium, Magadan province, northeastern Russia, is of great interest because of the occurrence of deposits of apparent "dropstones" and "ice rafted debris" that have been previously interpreted as glacial. Two high-precision U-Pb zircon ages, one for an intercalated volcanic tuff (262.5 ± 0.2 Ma) and the other for a boulder clast (269.8 ± 0.1 Ma) within a diamictite of the Atkan Formation, constrain the age of the Atkan Formation as Guadalupian (middle Permian). Sedimentologic study of the Atkan Formation casts doubt on the glacial nature of the diamictites. Deposition of rocks of the Atkan Formation temporally correlates with the Capitanian interglacial event in the southern hemisphere that recently was calibrated with high precision CA-TIMS. The previously proposed climate proxy record based upon warm-water foraminifera, which corresponds closely to global climate fluctuations, is compared with the glacial record of eastern Australia and indicates that the Capitanian was a time of globally warm climate. The sedimentology of Atkan Formation, the record of diversification of both fusulinids and rugosa corals, global sea-water temperature, and

sea-level fluctuations agree well with high latitude paleoclimate records in northeastern Russia and eastern Australia. Major components of the Atkan Formation, the volcanic rocks, are syngenetic with the sedimentation process. The volcanic activity in the nearby regions during middle-late Permian was quite extensive.

Key words: Guadalupian volcanism, Middle-Late Permian glaciation, U/Pb geochronology, Guadalupian climate, North-East Russia

1. Introduction

Bipolar ice caps are a main feature of many models for Earth's glaciations. For the late Paleozoic ice age, the evidence for bipolarity is not so obvious, although it is assumed in most publications (i.e., González and Díaz Saravia, 2010; Montanez and Poulson, 2013 and references there within). The Permian in northeastern Russia contains key sedimentary deposits that have been previously interpreted as glacial. The most cited glacial unit is the upper Permian Atkan Formation in Magadan province, northeastern Russia, and correlative units in the Omolon microcontinental block (Chumakov, 1994, 2015; Epshteyn, 1972; Raymond et al., 2004), where glacial deposits, including dropstones and ice rafted debris were reported (e.g., Epshtein, 1972; Chumakov 1994). These upper Permian deposits (in the older sense, but which now include middle [Guadalupian] and upper [Lopingian] Permian of the recent geologic time scale) have become the most commonly cited evidence for late Paleozoic glaciation in the Northern Hemisphere (Chumakov, 1994; Isbell et al., 2012; Montanez and Poulsen, 2013). Other Pennsylvanian and Cisuralian glacial deposits in northeastern Asia are very poorly documented or constrained (Ustritskiy and Yavshits, 1971).

Permian chronostratigraphy in northeastern Russia and correlative units outside of the region are still poorly defined due to an absence of diverse and high resolution conodont or fusulinid fossil faunas; the strong provinciality within other fossil faunas including brachiopods, bivalves, smaller foraminifera, and ammonoids; and a lack of radiometric dates. Although recent biostratigraphic studies have greatly improved the chronostratigraphy of these strata (Biakov, 2010; Davydov and Biakov, 2015, in press; Ganelin and Biakov, 2006; Karavaeva and Nestell, 2007; Klets et al., 2006; Kutygin et al., 2006), many problems remain in constraining the important paleobiologic and geologic events in this region. The presence of Permian volcanism is currently disputed by some geologists, and volcanic material, including boulders and gravel within the Atkan Formation, is interpreted as Devonian in age (Chumakov, 1994; Epshteyn, 1981; Ganelin, 1997, 2013). The new interpretations of the Atkan Formation as volcanoclastic diamictites (Biakov et al., 2010) provided an opportunity to apply recent geochemical methods, particularly U-Pb zircon geochronology, to resolve some of the chronostratigraphic problems mentioned above.

The Atkan Formation and similar diamictite-bearing sediments are widely distributed in northeastern Russia (Ganelin and Biakov, 2006; Biakov et al., 2010). In the Ayan-Yuryakh anticlinorium of the Magadan province, the formation hosts major gold deposits that include the giant Natalka deposit.

Here, we document the first high-precision chemical abrasion isotope dilution thermal ionization mass spectrometry (CA-TIMS) age for strata of the Atkan Formation using zircons collected from a volcanic ash bed and from a boulder contained within a "diamictite" (Fig. 1). These dates confirmed the widespread Permian volcanic activity in this and surrounding regions. The high precision U-Pb ages and sedimentologic nature of the Atkan diamictites also provide important constraints on regional and global paleoclimate interpretations.

2. Geologic setting

Northeastern Asia now consists of a complicated system of amalgamated allochthonous and autochthonous terranes. However, during the Permian, the region consisted of numerous developing sea and ocean basins (Parfenov et al., 1993; Shpikerman, 1998). A passive margin characterized the north-western (in paleo coordinates) border of the Siberian (North-Asian) Craton adjacent to the Verkhoyansk epicontinental sea along the passive margin of the Craton (Fig. 2). As much as 5.5 km of sedimentary successions deposited in this sea consist of relatively shallow-water, rhythmically- stratified siliciclastic deposits (Klets, 2005). To the northwest (in paleo coordinates), the Okhotsk Microcontinent comprised continental and shallow marine sedimentary deposits including abundant volcanic debris of various sizes and compositions (Umitbayev, 1963). Further west (in paleo coordinates), the Omolon Microcontinent was separated from the Siberian Craton and the Okhotsk Microcontinent by a series of deep-water basins including: 1) part of the Verkhoyansk epicontinental sea, 2) the Ayan-Yuryakh trough, and 3) the Balygychan and the Sugoy basins (Figs. 1-2). The Okhotsk-Taigonos volcanic arc (Biakov et al., 2005, 2007; synonymous with the Koni-Taigonos or Uda-Murgal arcs of Zaborovskaya, 1978; Nekrasov, 1976; Parfyonov, 1984) developed north and north-west of the basins and Okhotsk Microcontinent (Fig. 2). Rocks of this arc are composed of calc-alkaline volcanics (Umitbaev, 1963), with maximum eruptive activity having occurred during the Capitanian (Gizhigian) and continued volcanism that may have extended to the end of the Permian (Biakov, 2003; Biakov et al., 2005, 2010). The northwestern part of the arc likely developed upon the Okhotsk Microcontinent, whereas to the west, the Omolon Microcontinent was bounded by the deep-water Gizhiga and Taigonos basins (Umitbaev, 1963; Zhulanova et al., 1998).

3. Material

The Permian rocks described and analyzed in this paper were collected in the Natalka open-pit gold mine located in the southern part of the Yana-Kolyma fold belt on the southeastern flank of the Ayan-Yuryakh anticlinorium (Fig. 1). Here, the 5.5-km-thick Permian strata consist of the

Cisuralian and Guadalupian Pioneer, the Guadalupian Atkan, the Guadalupian to Lopingian Omchak, and the Lopingian Staratel' (Prospector) Formations (Biakov, 2007). At this locality, the Atkan Formation occurs on the limbs of the Natalka syncline, with rocks exposed along Geological Creek and the right bank of Natalka Creek at the margin of the mine pit (Fig. 1) that consist of the following 480-m-thick succession (from bottom to top):

1. Dark-grey massive diamictites with up to 1-m-thick layers of grey to light-grey fine-grained sandstone and silicic crystal tuffs (110 m)
2. Dark-grey massive diamictites (70 m)
3. Dark-grey massive diamictites intercalated with 1- to 25-m-thick, fine- to very fine-grained siltstones and 0.1- to 0.2-m-thick medium- to coarse-grained sandstones, with rare and thin horizons of silicic crystal tuffs (100 m)
4. Dark-grey massive diamictites (45 m)
5. Intercalations of dark-grey, fine- to very fine-grained siltstones, with rare beds of grey, medium- to coarse-grained sandstones (75 m)
6. Dark-grey massive diamictites (80 m)

Diamictites in the Atkan Formation are interbedded with thick, marine fossil-bearing graded sandstone and mudstone beds. The latter sometimes possessed deep-water trace fossils. Ripple marks and hummocky cross-stratification were not observed in the examined exposures. The diamictites are bedded. No striated or grooved surfaces were found beneath any of the units. The diamictites are matrix supported and vary from clast-poor to clast-rich deposits (cf. Hambrey and Glasser, 2012). Clasts are randomly dispersed throughout the diamictite and do not display preferred orientations, clast clustering, or striated and faceted surfaces.

The diamictites consist of mixed volcanic-siliciclastic debris, with volcanic components comprising from 10 to 50% of individual units (Biakov et al., 2010). The matrix of the diamictites consists of dark-grey, sericitized, silty-clay, with some sections transformed into a microfelsite aggregates with chaotically dispersed clasts ranging in size from granules to boulders. However, the vast majority of clasts fall within the granule to pebble size range. Granules contained within the matrix are partially composed of dacite and rhyolite. In thin-section, sand-sized particles (0.25-0.5 mm) dispersed in the matrix are angular to rounded and consist of equal amounts of volcanic quartz, plagioclase feldspar lathes, and larger lithic fragments. Approximately 50% of the lithic fragments consist of devitrified volcanic glass that has altered to a clay aggregate containing microfelsite crystals. Pumice debris, 0.2 -20 mm in diameter, with “torn” edges and occasional irregular “branchy” shapes, occur together with glassy palmate debris. Smaller grains of carbonate are also present.

Pebble to boulder-size clasts of volcanic rhyolite and dacite, and rare intrusive diorite and granodiorite, are unevenly distributed within the diamictites. Some boulders are as large as 0.7 m in diameter. A significant number of clasts, particularly the intrusive clasts, are well rounded, sometimes nearly isometric in shape, but the majority of the clasts (volcanic) have irregular shapes (Fig.3). Clasts displaying embayments and finger-like protrusions are common. Alteration hallows also surround some clasts. The magmatic clasts are “floating” in a fine-grained volcanic-siliciclastic matrix. Morphologically, the textures of these deposits closely resemble some glacigenic diamictites from Gondwana (cf. Fielding et al., 2008a; Isbell et al., 2013b; Jones and Fielding, 2004; Young, 2013).

An absence of wave indicators, the association of the diamictites with graded sandstone beds that are interpreted as deep water turbidites, the occurrence of marine fossils, and the occurrence of deep-water trace fossils within the diamictite-bearing successions suggest that the Atkan strata were deposited within a deep-water marine environment that was well below storm-wave base. Although these deposits were previously interpreted as having a glacigenic origin, glacial indicators, such as striations and faceted surfaces, were not observed on any of the clasts, and an absence of grooved and striated surfaces beneath the diamictites precludes a subglacial origin or an origin as iceberg-turbate features (cf. O'Brien and Christie-Blick, 1992; Woodworth-Lynas and Dowdeswell, 1994; Eyles et al., 2005; Vesely and Assine, 2014). An absence of clast clusters and an absence of observed lonestones (dropstones) within non-diamictite facies suggest that ice rafting was not a factor in deposition of these units (cf. Thomas and Connell, 1985; Gilbert, 1990). The bedded nature of the diamictites (less than 2 m thick), their occurrence as thick diamictite successions, and an absence of preferred orientation of clasts suggest deposition of these units as debris flows within sediment gravity-flow fans (cf. Mulder and Alexander, 2001; Haughton et al., 2009; Carto and Eyles, 2012). The predominance of volcanic clasts, volcaniclastic sand grains, and tuff/volcanic glass fragments within the matrix indicate a volcanic arc provenance (Biakov et al., 2010). The absence of bullet-shaped and striated clasts, the abundant of clasts with embayments and finger-like protrusions, and an abundance of glass shards and grains containing altered volcanic glass preclude a glacial origin. Volcanic grains displaying these shapes and compositions would not survive intense abrasion typical of subglacial environments or long-term chemical weathering of pre-existing sedimentary rocks. The composition and shape of the grains suggest derivation from active volcanic sources or volcanic sediments, and the presence of embayed clasts and alteration halos in the matrix surrounding clasts may have resulted from the incorporation of incandescent grains into the volcanic debris flows.

The magmatic clasts were historically considered as Devonian, although the exact age was never established. Recently, however, U-Pb SHRIMP zircon analyses from the Atkan Formation have yielded an age of 278.8±3 Ma (Biakov et al., 2010), for a sample collected from the matrix (unpublished data, A. Biakov). But the matrix in the Atkan diamictites consists of particles of various sizes, including volcanic clasts and microclasts of various compositions. Some of these particles are reworked volcaniclastic grains. Therefore, the zircon crystals analyzed by Biakov et al (2010) likely included detrital components, which suggest that the reported age may not be the depositional age of the Atkan Formation.

In this study, two samples were collected from the Atkan Formation. One sample was a light grey rhyolite boulder (10 x 20 cm) that was enclosed within a dark-grey volcanic-siliciclastic matrix (Fig. 3) collected in the lower part of the Atkan Formation at Geological Creek (Figs. 1, 3). The second sample was collected from strata in the middle part of the Atkan Formation exposed in the Natalkin – Glukharynyi Creek watershed. This sample was a whitish-pink crystal tuff (0.5 kg) of probable rhyolitic composition. The tuff is altered, and it was not possible to make a thin-section from the collected material (Fig. 3).

4. Results. U-Pb geochronology

The U-Pb dates were obtained by the CA-TIMS method on single zircon grains (Table 1). Zircon was separated from rocks using standard techniques, annealed in a muffle furnace at 900° for 60 hours, mounted in epoxy, and polished until the centers of the grains were exposed. Cathodoluminescence (CL) images were obtained with a JEOL JSM-1300 scanning electron microscope and Gatan MiniCL. Zircon grains selected on the basis of CL images were removed from the epoxy mounts and subjected to chemical abrasion in concentrated hydrofluoric acid at 180°C for 12 hours, after which they were rinsed, spiked with the EARTHTIME ET535 isotopic tracer, and totally dissolved. Further details of chemical separation and mass spectrometry have been published in Davydov et al. (2010) and Schmitz and Davydov (2012). The CA-TIMS U-Pb dates and uncertainties were calculated using the algorithms of Schmitz and Schoene (2007), EARTHTIME ET535 tracer solution values of $^{235}U/^{205}Pb$ = 100.233, and $^{233}U/^{235}U$ = 0.99506, and the U decay constants of Jaffey et al. (1971). The $^{206}Pb/^{238}U$ ratios and dates are reported as corrected for initial ^{230}Th disequilibrium.

Weighted mean $^{206}Pb/^{238}U$ dates were calculated from equivalent dates. Errors on the weighted mean dates are given as ± x (y) [z] , where x is the internal error based on analytical uncertainties only, including counting statistics, subtraction of tracer solution, and blank and initial common Pb subtraction; y includes the tracer calibration uncertainty propagated in quadrature; and z includes the ^{238}U decay constant uncertainty propagated in quadrature. All errors are reported at the 95% (2-sigma) confidence interval.

Nine zircon grains from the volcanic tuff sample 12VD105 were analyzed, the four youngest of which yielded equivalent $^{206}Pb/^{238}U$ dates with a weighted mean $^{206}Pb/^{238}U$ date of **262.45 ± 0.21** (0.24) [0.37] Ma (MSWD = 1.3, probability of fit = 0.27) interpreted as the eruption and depositional age of the tuff. Four other grains yielded $^{206}Pb/^{238}U$ dates up to 266.3 ± 0.8 Ma in age, and one grain yielded a $^{206}Pb/^{238}U$ date of 298.17 ± 0.26 Ma; all are interpreted as inherited grains.

Six zircon grains from the volcanic boulder epiclast sample 12VD108a were analyzed, all of which yielded equivalent $^{206}Pb/^{238}U$ dates with a weighted mean $^{206}Pb/^{238}U$ date of **269.80 ± 0.08** (0.1) [0.32] Ma (MSWD = 2.2, probability of fit = 0.05). This is interpreted as the volcanic crystallization and eruptive age of the epiclast.

5. Discussion

5.1 Atkan Formation and its relationship to Gondwana Glaciation

Our results indicate that contemporaneous volcanism was occurring during deposition of strata in the Atkan Formation and that reworking of these materials, as well as Guadalupian-age volcanic deposits, supplied detritus to depositional basins adjacent to the late Paleozoic Siberian Craton. These deposits formed in deep-water settings well below wave base as volcanic debris flows, rather than as glacial deposits as previously interpreted. A deep-water origin is indicated by a lack of storm or wave reworked deposits, the presence of deep-water trace fossils, and an association of the diamictites with sandstones deposited as turbidites. The bedded nature of the diamictites and the occurrence of randomly dispersed clasts within individual units suggest that these deposits formed as debris flows. The abundance of volcanic grains and glass shards, the occurrence of embayed clasts, and an absence of striated and faceted clasts all indicate that the sediment originated from erosion of a volcanic landscape, rather than as a product of glacial processes.

The age of the Atkan Formation was initially proposed as Upper Permian (*sensu lato*) (Epsteyn, 1981), which in 1981 included the Guadalupian (middle Permian) and Lopingian (upper Permian *sensu stricto*) of the modern Permian International Time Scale (Henderson et al., 2012). The extensive study of brachiopods and bivalves in recent years has provided better age constraints for the formation (Biakov, 2007). The Atkan Formation in the Ayan-Yuryakh trough is assigned to the *Maitaia bella* bivalve zone that corresponds to the lower Gizhigian regional stage of northeastern Russia (Fig. 1) (Biakov, 2010). The latter correlates with the Capitanian of the International Time Scale because of the occurrence of the ammonoid *Timorites,* together with Gizhigian bivalves and brachiopods in the Transbaikal region (Kotlyar et al., 2006).

Our CA-TIMS U-Pb zircon ages corroborate the Capitanian age of the Atkan Formation, with the volcanic tuff depositional age of 262.45 ± 0.21 Ma. The eplclastic volcanic detritus comprising much of the Atkan Formation is also middle Permian (latest Roadian), based upon the rhyolite boulder age of 269.90± 0.08 (Fig. 4).

The widely accepted model of late Paleozoic Gondwana glaciation, which was derived entirely from eastern Australia and extended to include purported glaciation in the Russian Far East, does not easily equilibrate with new global faunal and geochronological data. In eastern Australia, two glacial episodes were reported for Guadalupian Series strata: the P3 glaciation that extended from upper Kungurian through Roadian time, and the P4 glaciation that developed from late Wordian through the entire Capitanian (Fielding et al., 2008b; Isbell et al., 2012; Henry, 2013; Montanez and Poulsen, 2013). These middle Permian glaciations are interpreted to have been smaller than early Permian Asselian-early Sakmarian (P1-Gondwana wide glaciation) and late Sakmarian-Artinskian (P2- only known from Australia) glaciations (Fielding et al., 2008b; Isbell et al., 2012; Frank et al., 2015). The P2, P3, and P4 glaciations of eastern Australia occurred at a time when polar Gondwana was apparently ice-free (Isbell et al., 2012, 2013b).

A new high-precision U-Pb calibration of the middle-late Permian strata of eastern Australian has recently placed revised constraints on the P3 and P4 glacial events (Metcalfe et al., 2015). The P3 glacial episode is now known to extend between ca. 271 Ma and 263.5 Ma (lower Roadian to lower Capitanian; Fig. 5). The older limit of this glacial event is well constrained. The younger limit is somewhat conventional and approximately constrained with the age of 263.51 that came from the top of the mid-Capitanian Broughton Formation. The latter is interpreted to have been deposited at the short interglacial episode between P3 and P4 alpine glaciation (Metcalf et al., 2015).

The age of the P4 glaciation is taken here to extend from 260 to 254.5 Ma (early to middle Wuchiapingian, possibly includes the latest Capitanian). This event occurs on the International Chronostratigraphic Chart between what is interpreted as the Guadalupian-Lopingian mass extinction, which might occur slightly below the formal G-L boundary, and two established U-Pb ages, 255.26 Ma that is slightly older than the P4 glacial deposits and 253.38 slightly younger than the glacial deposits (Metcalf et al., 2015).

Original dating of the P3 and P4 glacial events of eastern Australia and the original purported age and interpretation of suggested glacial diamictites in Siberia suggested that the Capitanian was a cold interval in Earth history. Our new dates for the Atkan Formation and the new dates for middle and late Permian glaciation in eastern Australia now indicate that the deposition of rocks of the Atkan Formation was not coeval with the eastern Australian P3 or P4 glaciations, but rather occurred during the warm interval between the two glacial events. The interpretation of the Atkan diamictites as volcanic debris flows suggests that the Capitanian in the northern polar region was also a warm climate interval. Therefore, the nature and age of the Atkan Formation has far reaching significance for middle and late Permian climatic models. This significance is outlined and its relationship to other climate indicators is explored below.

5.2 Capitanian Climate

In the last decade, the Capitanian was traditionally considered as an interval of global cooling, the Kamura event, associated with a high positive value of $\delta^{13}C$ for the carbonate record (Isozaki, 2007). At first, it was interpreted to have started in the early Capitanian (low part of *Yabeina* zone) and lasted as long as 4–5 million years. As proposed (Isozaki et al., 2007), during this time the $\delta^{13}C$ carbonate value rose above +4.5‰ and reached the maximum of +7.0‰ within the *Yabeina* fusulinid Zone of the early-middle Capitanian. This cooling event, interpreted to have been caused by high biotic productivity, may have been coeval with a long-term cooling event, which induces the mass extinction at the end of middle Permian (Isozaki, 2007). This mass extinction mainly effected the symbiont-bearing faunas of the “tropical trio”, i.e. fusulinids Verbeekinidae, giant bivalves Alatoconchidae, and rugosa corals Waagenophyllidae (Isozaki and Aljinovic, 2009). In later studies, however, the beginning of Kamura cooling event was placed in the middle Capitanian and the latest Capitanian and Wuchiapingian was interpreted as being a globally warm interval (Isozaki et al., 2011). Kofukuda et al. (2014) indicated the Kamura cooling event was associated with a so-called “barren interval” and extinction interval in the Akasaka and Ishiyama limestone terranes of Japan that correspond only to the uppermost part of Capitanian. The duration of the Kamura event was originally proposed as 4-5 million years (Isozaki et al., 2007), but has not been re-assessed since that work. According to the Japanese sedimentological record, the "barren interval" might not be greater in duration than about 15 percent of the Capitanian (i.e. less than 1 million years; Kofukuda et al., 2014; Ota and Isozaki, 2006). In the marine record, the Kamura event is correlated to the P4 glaciation in the continental record of eastern Australia (Isozaki et al., 2011; Fielding et al., 2008; Kofukuda et al., 2014).

The lack of analyses on the dynamics of fusulinid evolution within the Capitanian, as mentioned in the studies described above (Isozaki et al., 2007 etc.), conceal the fact that the highest diversity among Capitanian fusulinids occurs at the end of the stage (Chedia, 1987; Davydov, 2014; Leven, 2003; Ozawa, 1987), where, following the logic of the progressive cooling development (Isozaki et al., 2007), the diversity should be the lowest. Another feature that is contradictory to the proposed extinction/cooling during the entire Capitanian is the existence of a diverse assemblage of fusulinids, including advanced neoschwagerinids such as *Lepidolina*, in southern China in the type section of the Capitanian-Wuchiapingian boundary (Penglangton section), up to the top of the Capitanian *J. granti*/*Clarkina postbittery hongshuensis* conodont zones (Shen et al., 2007; V.I. Davydov, unpub. data). In fact, the assemblage from the Laibin Limestone, which constitutes the upper 10 m within this 120-m-thick Capitanian succession, contained the greatest diversity among fusulinids in the entire section (Shen et al., 2007).

The P3 or P4 cold climatic episodes in southern Gondwana are well correlated with global warming and cooling episodes documented in the record of benthic warm-water foraminifera along the North American continental shelves (Davydov, 2014). The global climatic warming events are associated with diversity peaks and with migration events of warm-water fusulinids into temperate North American shelves. These warming events are proposed to have occurred in the late Artinskian, the late Kungurian, the Capitanian, and the Changhsingian (Fig. 5). The cooling events correspond with low taxonomic diversity in the North American foraminiferal record and are proposed to have occurred in the early Artinskian, the early Kungurian, the Roadian–early Wordian, and the early Wuchiapingian (Davydov, 2014). According to these data, Capitanian time was associated with a warm global climate that, in addition to fusulinid data, is also supported by data showing global reef expansion (Weidlich, 2002) and an increase in global diversity of rugosa corals (Fedorowski, 1989).

These data are consistent with the records from the type area of the Capitanian in Texas. During the Pennsylvanian and Permian, the North American shelves were located in tropical paleolatitudes. However, these shelves appear to have had temperate paleoclimates as indicated by significantly lower foraminiferal and coral diversity than correlative warm-water Tethyan faunas (Davydov 2014; Fedorowsky, 1997; Fedorowsky et al., 2009). Davydov (2014) proposed that the episodic appearances of Tethyan warm-water fusulinid faunal elements in North American shelves indicate paleoclimatic warming events, rising sea levels, and interregional migrations of these taxa in the region. The recent record from several sections and wells in western Texas shows that a prominent warming event and a major fusulinid migration to North America occurred in the middle-late Capitanian (Nestell et al., 2006). Tethyan fusulinids, such as *Yabeina*, *Pseudokahlerina*, *Paradoxiella*, *Reichelina*, *Codonofusiella*, *Rauserella,* and *Lanchichites,* and the very characteristic Tethyan smaller foraminifera *Abadehella,* have all been found above the *Yabeina* in Texas (Dunbar and Skinner, 1937; Skinner and Wilde, 1955; Nestell et al., 2006). Neoschwagerinids, including *Yabeina*, are climatically sensitive foraminifera that survive only in very warm paleoenvironments where surface waters are thought to have exceeded an annual temperature of 20–22 °C (Ueno, 2006; Davydov and Arefifard, 2013). It seems that the shallow-water paleoclimatic condition in Texas at that time was marginal for neoschwagerinids, as *Yabeina* is rare in the area and is represented by a small and primitive form. The remainder of the fusulinids, i.e., schubertellids schwagrinids and ozawainellids, survive into more temperate environments (Davydov, 2011, 2014; Davydov and

Arefifard, 2013). *Polydiexodina* predominates among fusulinids in the lower-middle Capitanina in Texas (Wilde, 2000). The morphologic and environmental similarity of *Eoparafusulina*, *Monodioexodina,* and *Polydiexodina* (Davydov, 2014; Davydov and Arefifard, 2013; Ueno, 2006) also suggests a more temperate climate in the early-middle Capitaninin of Texas. The Texas fusulinids generally show increased diversity towards the end of the Capitanian (Nestell and Nestell, 2006), and therefore suggest a progressive warming rather than cooling trend at that time. The extinction episode in Texas occurs in the latest Capitanian between middle and upper Tonsil Members (Nestell and Nestell, 2006) and at the top of Reef Trail Formation (Wilde et al., 1999), near the top of the global Capitanian Stage, and the top of the *Jinogondolella granti* and *Clarkina postbittery hongshuensis* conodont zones (Nestell and Wradlaw, 2010). We consider the idea that the fusulinid genera that are all known in the *J. granti* conodont Zone also occur in Wuchiapingian strata elsewhere in the world (Bond et al., 2010) to be incorrect, because of a lack of an supporting data for such conclusion (Davydov and Arefifard, 2013; Kobayashi, 2012; Kofukuda et al., 2014; Kolodka et al., 2012; Wingall et al., 2012). For the Capitanian, a strong link between biotic and climatic events in North America, and the similarity of biotic changes between the North American and other regions, suggests that paleoclimatic events within the North America were controlled by global factors (Davydov, 2014).

The data from Zagros sections in Iran are also consistent with the latter observation (Davydov and Arefifard, 2013). Warm-water Neoschwagerinids *Afghanella* and *Sumatrina* in the region occur in late Capitanian, whereas temperate *Chusenella*, *Eoplydiexodina,* and *Monodiexodina kattaensis* are documented in the early Capitanian (Davydov and Arefifard, 2013). Similarly, in Transcaucasia, the fusulinids from the lower Midian substage (analogue of upper Wordian) consists of predominantly schubertellids, ozawainellids, and endemic schwagerinids, whereas in the upper Midian (e.g., Capitanian) *Neoschwagerina* and abundant *Kahlerina* are present (Kotlyar et al., 1989).

The essentially complete Wordian-Wuchiapingian shallow carbonates succession has been described lately in the north-east Thailand (Hada et al., 2015). The Capitanian there assigned to the *Lepidolina* fusulinid zone divided into two units. Unit one characterized by relatively diverse assemblage including *Sumatrina annae* (Volz), *S. longissima* (Deprat), Neoschwagerina craticulifera (Schwager), Yabeina cf. globosa (Yabe), Lepidolina asiatica (Ishii) and L. columbiana (Dawson). However, upper unit (two) contains very diverse assemblage of several *Lepidolina*, *Verbeekina*, *Codonofusiella* and *Dunbarula* species. Besides, the abundant green algae *Mizzia*, *Macroporella* and *Gymnocodium* along with extraordinarily large Alatoconchidae bivalves documented in the uppermost Capitanian (Hada et al., 2015). Therefore, again as in the other regions the most abundant and warmest assemblage of fusulinids, algae and bivalves occur in the upper Capitanian.

Recently, the Kamura event has been recognized in the Chandalaz regional stage in southern Primorie, Russian Far East (Kossovaya and Kropacheva, 2013) and is correlative to the Capitanian of the International Time Scale. The $\delta^{13}C$ carbonate isotopic signature within the limestone succession of the Chandalaz Formation interpreted as the evidence of the Kamura cooling event. The fusulinids in the *Monodiexodina sutchanica-Metadoliolina dutkevitchi* zone of the lower Chandalaz Formation consist predominantly of temperate *Monodiexodina* and rare *Metadoliolina, Parafusulina, Pseudofusulina, Chusenella, Minojapanella, Codonofusiella, Sichotenell, Rauserella,* and *Reichelina*. Single and incomplete specimens of neoschwagerinids (*Colania*/*Lepidolina*) are found near the top of this zone (Chedia in Kotlar et al., 1989; V.I. Davydov, unpub. data). Fusulinid diversity increases dramatically in the overlying *Parafusulina stricta* zone, where neoschwagerinids *Lepidolina,* including *L. kumaensis,* become common (Fig. 6). The dominant taxa there are *Parafusulina*, *Pseudofusulina*, *Skinerella*, *Chusenella*, and numerous and diverse schubertellids and ozawainellids. In the upper part of the Chandalaz fusulinid zone, *Metadoliolina lepida- Lepidolina kumaensis*, the neoschwagerinds, are the dominant element of the assemblage. They include *Lepidolina*, *Neosumatrina*, *Yabeina,* and *Neoschwagerina*. The verbikiinids, schwagerinids, schubertellids, and ozawainellids are exceptionally diverse (Chedia, 1981; Chedia in Kotlar et al., 1989; Sosnina, 1981, 1983). Thus, the fusulinids in Primorie are characterized by the same trend in diversity increase towards the end of the Capitanian as those in Texas, Transcaucasia, Zagros, and southern China.

Similar to the fusulinids, the rugosa corals in southern Primorie in the lower Chandalaz Formation *Monodiexodina sutchanica-Metadoliolina dutkevitchi* fusulinid zone, are represented by the solitary form only and their diversity there is low (Kossovaya and Kropacheva, 2013). Solitary corals appear in a wide range of the climatic environments from temperate to very warm, whereas massive colonial corals exist only in predominantly warm climate (Fedorovsky et al., 2007; Kossovaya and Kropacheva, 2013). A dramatic increase in coral diversity occurs in the *Parafusulina stricta* fusulinid zone. Rare massive colonial forms were found in the upper part of this fusulinid zone (Figure 6). The latter corals predominate in the *Metadoliolina lepida-Lepidolina kumaensis* fusulinid zone (Kossovaya and Kropacheva, 2013). Only rare solitary corals are present in the uppermost part of the Chandalaz succession where fusulinids are absent. This part of the succession reasonably correlates with the "barren interval" of the topmost Capitanian Kamura event in Japan (Kossovaya and Kropacheva, 2013). The diversity data of rugosa corals in the Capitanian of Primorie are consistent with the overall diversity trends throughout Tethys (Fedorovsky, 1997) (Figure 6).

The trend of increasing faunal diversification throughout the Capitanian and the appearance of warm-water massive colonial corals (i.e., *Waagenophyllidae*) and tropical reefs in the upper Capitanian *Metadoliolina lepida- Lepidolina kumaensis* fusulinid zone are inconsistent with the suggested Kamura cooling event at that time (Kossovaya and Kropacheva, 2013). This contradiction could be explained by southward movement of the Primorie terranes during the Capitanian (Kossovaya and Kropacheva, 2013). However, most of the widely accepted paleogeography maps (Boucot et al., 2013; Golonka, 2011; Lawver et al., 2011; Scoteese, 2014) suggest stable or northward movement of the terranes during Cisuralian and Guadalupian. In addition, southward movement that would be great enough to cause warming of at least 4-5 °C (low diversity solitary forms in *Monodiexodina sutchanica-Metadoliolina dutkevitchi* fusulinid zone ***vs*** dominance of massive colonial forms in zone *Metadoliolina lepida-Lepidolina kumaensis* fusulinid zone) in deep-slope temperate water environments and habitats of the Primorie corals (Kossovaya and Kropacheva, 2013) would require southward movement of at least 1500-2000 km during the Capitanian (Montanez and Poulsen, 2013). This is unrealistic as it is more likely that the late Capitanian fusulinid and coral diversification was associated with late Capitanian climate warming.

Recent studies $\delta^{18}O$ isotopes from biogenic carbonates in the low, middle and high latitudes (Korte et al., 2008) clearly suggest a global cooling phase during Roadian time and then the subsequent progressive warming from Wordian towards the end of the Capitanian. High-resolution oxygen isotope data for the entire Permian, with ages based on the several hundred conodont biogenic apatite dates from low latitude locations in southern China, Iran, and Texas, USA, provide a unique late Paleozoic paleotemperature and ice volume history on a global scale (Chen et al., 2013). This record shows significant surface temperature fluctuation within the Guadalupian-Lopingian transition, with a 4 °C warming in the late Capitanian, followed by 6 to 8 °C cooling during the early Wuchiapingian. This cooling is interpreted as a combined climate change signature initiated by Emeishan volcanism and changes in the habitat depth of gondolellid conodonts as a consequence of sea-level changes (Chen et al., 2013). The global eustatic sea-level variations (Rigel et al., 2008) are not always supported by the paleoclimate model proposed here, mostly because of less reliable chronostratigraphic constraints that require further study. The biogenic conodont apatite geochemical data are consistent with the glaciation-deglaciation records and recent data from eastern Australia (Metcalfe et al., 2015) and the model proposed here.

6. **Conclusions**:

1. High-precision U-Pb zircon dates for the Atkan Formation in the Ayan-Yuryakh anticlinorium, Magadan province, northeastern Russia verify a Capitanian depositional age, and support intensive volcanic activity in the region during Guadalupian time.
2. The sedimentology of the Atkan Formation casts doubt on the glacial nature of the diamictites.
3. The Capitanian was most likely a time of global warming, based upon the new available high-precision U-Pb zircon ages of the eastern Australian glacial record and available geochemical data.
4. The diversification of fusulinids and corals increased from the early Capitanian towards the end of the stage. This correlates with the migration event of warm water neoschwagerinid fusulinids and massive colonial rugosa corals into temperate North America shelf basins and it agrees well with high-latitude paleoclimate records in northeastern Russia and eastern Australia.
5. The conodont biogenic apatite isotopic data agree with biota and glacial records and suggest a warming trend occurred from early-middle Guadalupian to the end of the Capitanian.

Acknowledgements.

This paper was completed with support from NSF grants EAR-1124488, a seed grant from the University of Wisconsin-Milwaukee’s Research Grant Initiative (RGI) and the Russian Foundation for Basic Research, project no. 14-05-00217 (to ASB). The research was also funded in part by the subsidy of the Russian Government to support the Program of Competitive Growth of Kazan Federal University among the World Leading Academic Centers. We thank E.V. Kolesov and Yu. Yu. Ivanov for their assistance in the field. The notes and suggestions of Prof. Metcalfe and the Editor Richard Goldfarb are greatly improved the manuscript.

Figures and tables capture.

Table 1 U-Pb isotopic CA-TIMS data from samples 12VD105 and 12VD108.

Fig. 1. Generalized Permian and Lower Triassic succession and location of the Ayan-Yuryakh Basin in the tectonic montage of the Yana-Kolyma folded system in northeastern Russia (after Shpikerman, 1998; Biakov, 2006).

Fig. 2. Paleogeographic map of the globe during the Lopingian (Lawver et al., 2011). Main cratons include: AFR, Africa; AMR, Amuria; BAL, Baltica; GR, Greenland; NAM, North America; NCB, North China Block; SIB, Siberia. High-latitude northern terranes and arcs: AOA, Alazeay-Oloi Arc System; OB, Omulevka Block; OK, Okhotsk Block; OM, Omolon Microcontinent; OTA, Okhotsk-Taigonos Arc system; VB, Verkhoyansk epicontinental sea.

Fig. 3. Photos of rock and strata exposed around the Natalka gold mine. 3A, general view of the Natalka gold mine, red arrow shows the approximate position of the volcanic ash (sample 12VD105) from which zircons were obtained for dating; 3B, the rhyolite volcanic boulder epiclast (sample 12VD108) within Atkan diamictite rock; 3C, cross-cut of the boulder; 3D and 3F, semi-altered volcanic ash (sample 12VD105).

Fig. 4. Plot of $^{206}Pb/^{238}U$ dates from single grains of zircon analyzed by CA-TIMS. Plotted with Isoplot 3.0 (Ludwig, 2003). Error bars are at the 2-sigma confidence interval. A weighted mean date is shown and represented by the grey boxes behind the error bars. One older date from 12VD105 is not shown.

Fig. 5. Warming and cooling events along the North American shelves during late Cisuralian through the end of the Permian. The warming events associated with diversity peaks and occur in late Artinskian, late Kungurian, Capitanian, and Changhsingian. The cooling events correspond to low taxonomic diversity interval and proposed to occur in early Artinskian, early Kungurian, Roadian–early Wordian, and early Wuchiapingian (from Davydov, 2014). Radiometric calibration of P3 and P4 glacial events of Australia from Metcalfe et al., 2015. The age of the volcanic tuff from the middle Atkan Formation is slightly younger the age 263.51 from the top of mid-Capitanian Broughton Formation that is interpreted as the short interglacial episode between P3 and P4 alpine glaciation (Metcalfe et al., 2015). Abbreviations for the chronostratigraphic units: Lnx—lower part of Lenoxian. Word.—Wordian; Changhsin—Changhsingian. P2 glacial event (Artinskian-Kungurian) cited in the literature as a single glaciation, whereas fusulinid record suggests a global warming climatic episode in late Artinskian. Therefore, it is proposes the existence of two glacial episodes that are not yet recognized as separate. The late Artinskian warming spike is derived from fusulinid data from Urals, North America shelves, Timor, and Thailand (Davydov et al., 2013; Davydov, 2014; Ueno et al., 2015).

Fig. 6. Biota (fusulinid and rugosa corals), conodont biogenic apatite geochemistry, global eustatic sea-level and radiometric calibration constrains in regards of the recognized paleoclimatic events and proposed here. Fusulinid data and paleoclimate interpretations from Davydov, 2014. For more explanations see figure 5. Tethyan rugosa corals diversity from Fedorovsky, 1997 and Wang and Sugiyama, 2002. Two diversity peaks in Rugosa generally corresponds with late Artinskian and middle-late Capitanian fusulinids diversity maximum, although the chronostratigraphic constrains on the corals are not as accurate as on fusulinids and thus, the diversity pattern is more generalized. The details of the Capitanian rugosa record (selected by the dashed lines) are from the Primorye region (Kossovaya and Kropacheva, 2013)

as the records from other areas are lacking this information. The dominance of massive colonial forms (*Szechuanophyllum kitakamiense–Wentzelloides* ussuricus coral zone) corresponds with highest diversity among fusulinids in both Texas and Primorie regions (see details in the text). The biogenic apatite geochemical sea-water temperature from Chen et al., 2013 and the global eustaic sea-level frequency and magnitude is from Rigel et al., 2008. The paleotemperature and global sea-level fluctuations show general trend from ice house to greenhouse global climate. Sharp early Wuchiapingian sea water temperature drop (Chen et al., 2013) coincided with P4 glacial event in eastern Australian. The global eustatic sea-level variations (Rigel et al., 2008) are not always supported the proposed paleoclimate model because of less reliable chronostratigraphy constrains on the sea level curve, which require further updates. Conodont abbreviations: *C. – Clarkina; J. - Jinogondolella*

References

Biakov, A.S., 2006. Permian bivalve mollusks of Northeast Asia. Journal of Asian Earth Sci-ences (ISSN: 1367-9120) 26 (3–4), 235–242. http://dx.doi.org/10.1016/j.jseaes.2005. 11.005

Biakov, A.S., 2007. Permian biostratigraphy of the Northern Okhotsk Region (Northeast Asia). Stratigraphy and Geological Correlation 15 (2), 161–184.

Biakov, A.S., 2010. Zonal stratigraphy, event correlation, paleobiogeography of the Permian of Northeast Asia (based on bivalves). In: Chuvashov, B.I. (Ed.), NEISRI FEB RAS, Magadan. ISBN: 978-5-94729-102-5 (in Russian with English summary).

Biakov, A.S., Vedernikov, I.L., Akinin, V.V., 2010. Permian diamictites of North-East Asia and their probable origin. News of North-Eats Scientific Center of Russian Academy of Sciences, 14-24 (in Russian with English abstract).

Boucot, A.L., Xu, Chen , and Scotese, Ch. R., 2013. Phanerozoic Paleoclimate: An Atlas of Lithologic Indicators of Climate. SEPM (Society for Sedimentary Geology).

Carto, S.L., Eyles, N., 2012. Identifying glacial influences on sedimentation in tectonically-active, mass flow dominated arc basins with reference to the Neoproterozoic Gaskiers glaciation (c. 580 Ma) of the Avalonian-Cadomian orogenic belt. Sedimentary Geology 261-262, 1-14.

Chediya, I.O., 1981. Important criteria the species designation of Lepidolina genus (Neoschwagerinidae family). Voprosy micropaleontologii 24, 60-75 (In Russian).

Chen, B., Joachimski, M.M., Shen, S., Lambert, L.L., Lai, X., Wang, X., Chen, J., Yuan, D., 2013. Permian ice volume and palaeoclimate history; oxygen isotope proxies revisited. Gondwana Research 24, 77-89.

Chumakov, N.M., 1994. Evidence of Upper Permian glaciation on the Kolyma River; repercussions of the Gondwana glaciation in northeastern Asia? Stratigrafiya Geologicheskaya Korrelyatsiya 2, 130-150 (in Russian)

Chumakov, N.M., 2015.The role of glaciations in the biosphere. Russian Geology and Geophysics 56, 541–548.

Davydov, V.I., 2014. Warm water benthic foraminifera document the Pennsylvanian–Permian warming and cooling events — The record from the Western Pangea tropical shelves. Palaeogeography, Palaeocimatology and Palaeogeography 414, 284-295.

Davydov, V.I., 2011. Taxonomy, nomenclature and evolution of the early schubertellids (Fusulinida, Foraminifera) Acta Palaeontologica Polonica. 56, 181-194.

Davydov, V.I., Arefifard, S., 2013. Middle Permian (Guadalupian) fusulinid taxonomy and biostratigraphy of the mid-latitude Dalan Basin, Zagros, Iran and their applications in paleoclimate dynamics and paleogeography. Geoarabia 18, 17-62.

Davydov, V.I., Biakov, A.S., 2015 (in press). Discovery of shallow-marine biofacies conodonts in a bioherm within the Carboniferous–Permian transition in the Omolon Massif, NE Russia near the North paleo-pole: Correlation with a warming spike in the southern hemisphere. Gondwana Research, 10.

Davydov, V.I., Haig, D.W., McCartain, E., 2014. Latest Carboniferous (late Gzhelian) fusulinids from Timor Leste and their paleobiogeographic affinities. Journal of Paleontology 88, 588-605.

Dunbar, C.O., Skinner, J.W., 1937. Permian Fusulinidae of Texas. University of Texas Bulletin, Report 3701, 517-825.

Epshteyn, O.G., 1972. Upper Permian glacial marine deposits in the source basin of the Kolyma River. Litologiya i Poleznyye Iskopayemyye 3, 112-127(in Russian).

Epshteyn, O.G., 1981. Late Permian ice-marine deposits of the Atkan Formation in the Kolyma River headwaters regions, U.S.S.R, In: Hambrey, M.J., Harland, W.B. (Eds.), Earth's Pre-Pleistocene Glacial Record. Cambridge University Press, Cambridge, U.K., pp. 270-273.

Eyles, N., Eyles, C.H., Woodworth-Lynas, C., Randall, T.A., 2005. The sedimentary record of drifting ice (early Wisconsin Sunnybrook deposit) in an ancestral ice-dammed Lake Ontario, Canada. Quaternary Research 63, 171-181.

Fedorowski, J., 1989. Extinction of Rugosa and Tabulata near the Permian Triassic boundary. Memoir of the Association of Australasian Palaeontologists 8, 346.

Fedorowski, J., Bamber, W.E., Stevens, C.H., 2007. Lower Permian Colonial Rugose Corals, Western and Northwestern Pangaea: Taxonomy and Distribution. NRC Research Press,, Ottawa, Ontario, Canada.

Fedorowski, J., Bamber, W.E., Stevens, C.H., 1999. Permian corals of the Cordilleran-Arctic-Uralian Realm. Acta Geologica Polonica 49, 159-173.

Fielding, C.R., Frank, T.D., Birgenheier, L.P., Rygel, M.C., Jones, A.T., Roberts, J., 2008a. Stratigraphic record and facies associations of the late Paleozoic ice age in eastern

Australia (New South Wales and Queensland). Special Paper - Geological Society of America 441, 41-57.

Fielding, C.R., Frank, T.D., Isbell, J.L., 2008b. The late Paleozoic ice age; a review of current understanding and synthesis of global climate patterns. Special Paper - Geological Society of America 441, 343-354.

Frank, T.D., Shultis, A.I., Fielding, C.R., 2015. Acme and demise of the late Palaeozoic ice age: A view from the southeastern margin of Gondwana. Palaeogeography, Palaeoclimatology, Palaeoecology 418, 176-192.

Ganelin, V.G., 1997. Boreal benthic biota in the structure og the Late Paleozoic World Ocean. Stratigrafiya Geologicheskaya Korrelyatsiya 5, 29-42 (in Russian).

Ganelin, V.G., 2013. Middle-to-late Paleozoic transition, late Paleozoic sedimentation and biocenoses in northeastern Asia. Geokart, Moscow(in Russian).

Ganelin, V.G., Biakov, A.S., 2006. The Permian biostratigraphy of the Kolyma-Omolon region, Northeast Asia. Journal of Asian Earth Sciences 26, 225-234.

Gilbert, R., 1990. Rafting in glacimarine environments, In: Dowdeswell, J.A., Scourse, J.D. (Eds.), Glacimarine environments: processes and sediments. Geological Society Special Publications, pp. 105-120.

Golonka, J., 2011. Phanerozoic palaeoenvironment and palaeolithofacies maps of the Arctic region, In: Spencer, A.M., Embry, A.F., Gautier, D.L., Stoupakova, A.V., Sorensen, K. (Eds.), Memoirs of the Geological Society of London. Geological Society of London, London, London, pp. 79-129.

Hada, S.,Khosithanont, S., Goto, H., Fontaine, H. and Salyapongse, S., 2015.Evolution and extinction of Permian fusulinid fauna in the Khao Tham Yai Limestone in NE Thailand. Journal of Asian Earth Sciences, 104, 175–184.

Haughton, P., Davis, C., McCaffrey, W., Barker, S., 2009. Hybrid sediment gravity flow deposits; classification, origin and significance. Marine and Petroleum Geology 26, 1900-1918.

Henderson, C., Davydov, V.I., Wardlaw, B.R., 2012. The Permian Period, In: Gradstein, F.M., Ogg, J.G., Schmitz, M.D., Ogg, G. (Eds.), The Geologic Time Scale 2012. Elsevier, Amsterdam, pp. 653-679.

Henry, L.C., 2013. Late Paleozoic glaciation and ice sheet collapse over Western and Eastern Gondwana: Sedimentology ad Stratigraphy of glacial to post-glacial strata in Western Argentina and Tasmania, Australia, Geosciences. The University of Wisconsin-Milwaukee, Wisconsin-Milwaukee, p. 313.

Isbell, J.L., Biakov, A.S., Vedernikov, I.L., Davydov, V.I., Gulbranson, E.L., Fedorchuk, N.D., Kolesov, E.V., Ivanov, Y.Y., 2013a. Reevaluation of Permian glaciation in Siberia during the late Paleozoic ice age; preliminary analyses on the origin of capitanian diamictites in the Atkan formation, Okhotsk region, Russia. Abstracts with Programs - Geological Society of America 45, 301.

Isbell, J.L., Gulbranson, E.L., Taboada, A.C., Pagani, M.A., Limarino, C.O., Fraiser, M.L., Pauls, K.N., Henry, L.C., 2013b. Carboniferous and Permian strata of the Tepuel-Genoa Basin, Patagonia, Argentina; a near-continuous, deep-water record of polar Gondwana during the late Paleozoic ice age. Bulletin - New Mexico Museum of Natural History and Science 60, 137-138.

Isbell, J.L., Henry, L.C., Gulbranson, E.L., Limarino, C.O., Fraiser, M.L., Koch, Z.J., Ciccioli, P.L., Dineen, A.A., 2012. Glacial paradoxes during the late Paleozoic ice age; evaluating the equilibrium line altitude as a control on glaciation. Gondwana Research 22, 1-19.

Isozaki, Y., Aljinovic, D., 2009. End-Guadalupian extinction of the Permian gigantic bivalve Alatoconchidae; end of gigantism in tropical seas by cooling. Palaeogeography, Palaeoclimatology, Palaeoecology 284, 11-21.

Isozaki, Y., Aljinovic, D., Kawahata, H., 2011. The Guadalupian (Permian) Kamura event in European Tethys. Palaeogeography, Palaeoclimatology, Palaeoecology 308, 12-21.

Isozaki, Y., Kawahata, H., Ota, A., 2007. A unique carbon isotope record across the Guadalupian-Lopingian (Middle-Upper Permian) boundary in mid-oceanic paleo-atoll carbonates; the high-productivity "Kamura event" and its collapse in Panthalassa. Global and Planetary Change 55, 21-38.

Jones, A.T., Fielding, C.R., 2004. Sedimentological record of the late Paleozoic glaciation in Queensland, Australia. Geology 32, 153-156.

Karavaeva, N.I., Nestell, G.P., 2007. Permian foraminifers of the Omolon Massif, northeastern Siberia, Russia. Micropaleontology 53, 161-211.

Klets, A.G., 2005. Upper Paleozoic of the Angarida marginal seas. GEO, Novosibirsk(in Russian).

Klets, A.G., Budnikov, I.V., Kutygin, R.V., Biakov, A.S., Grinenko, V.S., 2006. The Permian of the Verkhoyansk-Okhotsk region, NE Russia. Journal of Asian Earth Sciences 26, 258-268.

Kofukuda, D., Isozaki, Yu., Igo, H. 2014. A remarkable sea-level drop and relevant biotic responses across the Guadalupian–Lopingian (Permian) boundary in low-latitude mid-Panthalassa: Irreversible changes recorded in accreted paleo-atoll limestones in Akasaka and Ishiyama, Japan Journal of Asian Earth Sciences 82 (2014) 47–65.

Kolodka, C., Vennin, E., Vachard, D., Trocme, V., Goodarzi, M.H., 2012. Timing and progression of the end-Guadalupian crisis in the Fars province (Dalan Formation, Kuh-e Gakhum, Iran) constrained by foraminifers and other carbonate microfossils. Facies 58, 131-153.

Korte, C., Jones, P.J., Brand, U., Mertmann, D., Veizer, J., 2008. Oxygen isotope values from high-latitudes: clues for Permian sea-surface temperature gradients and Late Palaeozoic deglaciation. Palaeogeography, Palaeoclimatology, Palaeoecology 269, 1–16.

Kossovaya, O.L., Kropatcheva, G.S., 2013. Extinction of Guadalupian rugose corals; an example of biotic response to the Kamura event (southern Primorye, Russia). Special Publication - Geological Society of London 376.

Kotlyar, G.V., Zakharov, Y.D., Kropacheva, G.S., Pronina, G.P., Chedija, I.O., Burago, V.I., 1989. Evolution of the latest Permian Biota. Midian regional stages in the USSR. Nauka, Leningrad.

Kotlyar, G.V., Popeko, L.I., Kurilenko, A.V., 2006. The Permian of the Transbaikal region, eastern Russia; biostratigraphy, correlation and biogeography. Journal of Asian Earth Sciences 26, 269-279.

Kutygin, R.V., 2006. Permian ammonoid associations of the Verkhoyansk region, Northeast Russia. Journal of Asian Earth Sciences 26, 243-257.

Lawver, L.A., Gahagan, L.M., Norton, I., 2011. Palaeogeographic and tectonic evolution of the Arctic region during the Palaeozoic. Memoirs of the Geological Society of London 35, 61-77.

Leven, E.Y., 2003. Dinamika rodovogo raznoobraziya i osnovnyye etapy evolyutsii fuzulinid. Fusulinidae diversity dynamics and main stages of evolution. Stratigrafiya, Geologicheskaya Korrelyatsiya 11, 15-26.

Metcalfe, I., Crowley, J.L., Nicoll, R.S., Schmitz, M., 2015 in press. High-precision U-Pb CA-TIMS calibration of Middle Permian to Lower Triassic sequences, mass extinction and extreme climate-change in eastern Australian Gondwana. Gondwana Research.

Montanez, I.P., Poulsen, C.J., 2013. The late Paleozoic ice age; an evolving paradigm. Annual Review of Earth and Planetary Sciences 41, 629-656.

Mulder, T., Alexander, J., 2001. The physical character of subaqueous sedimentary density flows and their deposits. Sedimentology 48, 269-299.

Nestell, M.K., Nestell, G.P., Wardlaw, B.R., Sweatt, M.J., 2006. Integrated biostratigraphy of foraminifers, radiolarians and conodonts in shallow and deep water Middle Permian (Capitanian) deposits of the "Rader slide", Guadalupe Mountains, West Texas. Stratigraphy 3, 161-194.

Nestell, M.K., Wardlaw, B.R., 2010. Radiolarians and conodonts of the Guadalupian (Middle Permian) of West Texas; advances in taxonomy and biostratigraphy. Micropaleontology 56, 1-6.

O'Brien, P.E., Christie-Blick, N., 1992. Glacially grooved surfaces in the Grant Group, Grant Range, Canning Basin and the extent of Late Paleozoic Pilbara ice sheets. BMR Journal of Australian Geology and Geophysics 13, 87-92.

Ota, A., Isozaki, Y., 2006. Fusuline biotic turnover across the Guadalupian–Lopingian (Middle-Upper Permian) boundary in mid-oceanic carbonate buildups: biostratigraphy of accreted limestone in Japan. J. Asian Earth Sci. 26, 353–368.

Ozawa, T., 1987. Permian fusulinacean biogeographic provinces in Asia and their tectonic implications. Terra Sci. Publ. Co., Tokyo.

Parfenov, L.M., Natapov, L.M., Sokolov, S.D., Tsukanov, N.V., 1993. Terranes and Accretionary Tectonics of Northeastern Asia. Geotectonics 27, 62-72 (in Russian).

Raymond, A.L., Metz, C., Parrish, J.T., 2004. Ice and its consequences; glaciation in the Late Ordovician, Late Devonian, Pennsylvanian-Permian, and Cenozoic compared, Journal of Geology, pp. 655-670.

Rygel, M.C., Fielding, C.R., Frank, T.D., Birgenheier, L.P., 2008. The magnitude of late Paleozoic glacioeustatic fluctuations; a synthesis. Journal of Sedimentary Research 78, 500-511.

Scotese, C.R., 2014. Atlas of Permo-Carboniferous Paleogeographic Maps (Mollweide Projection), Maps 53 – 64, Volumes 4, The Late Paleozoic, PALEOMAP Atlas for ArcGIS, PALEOMAP Project, Evanston, IL.

Shen, S.-Z., Wang, Y., Henderson, C.M., Cao, C.-Q., Wang, W., 2007. Biostratigraphy and lithofacies of the Permian System in the Laibin-Heshan area of Guangxi, South China. Palaeoworld 16, 120-139.

Shpikerman, V. I., 1998. Pre-Cretaceous minerageny of the North-East Asia. NEISRI FEB RAS, Magadan (in Russian).

Skinner, J.W., Wilde, G.L., 1955. New fusulinids from the Permian of West Texas. Journal of Paleontology 29, 927-940.

Sosnina, M.I., 1981. Nekotoryye permskiye fuzulinidy Dal'nego Vostoka. Some Fusulinida of the Permian of the Far East. Ezhegodnik Vsesoyuznogo Paleontologicheskogo Obshchestva 24, 13-34.

Sosnina, M.I., 1983. Nekotoryye novyye predstaviteli miliolid i nodozariid pozdney permi Yuzhnogo Primor'ya (foraminifery). Some new miliolids and nodosarids of the Upper Permian of South Primorye; foraminifera. Ezhegodnik Vsesoyuznogo Paleontologicheskogo Obshchestva 26, 29-47.

Thomas, G.S.P., Connell, R.J., 1985. Iceberg drop, dump, and grounding structures from Pleistocene glacio-lacustrine sediments, Scotland. Journal of Sedimentary Petrology 55, 243-249.

Ueno, K., Arita, M., Meno, S., Sardsud, A., Saesaengseerung, D., 2015, in press. An Early Permian fusuline fauna from southernmost Peninsular Thailand: Discovery of Early Permian warming spikes in the peri-Gondwanan Sibumasu Block. Journal of Asian Earth Sciences, 104, 185–196.

Ueno, K., 2006. The Permian antitropical fusulinoidean genus Monodiexodina; distribution, taxonomy, paleobiogeography and paleoecology. Journal of Asian Earth Sciences 26, 380-404.

Ueno, K., Arita, M., Meno, S., Sardsud, A., Saesaengseerung, D., 2015, in press. An Early Permian fusuline fauna from southernmost Peninsular Thailand: Discovery of Early Permian warming spikes in the peri-Gondwanan Sibumasu Block. Journal of Asian Earth Sciences, 12 pages.

Ustritskiy, V.I., Yavshits, G.P., 1971. Middle Carboniferous glaciomarine sediments in the northeastern USSR. Doklady Akademii Nauk SSSR 199, 437-440(in Russian).

Vesely, F., Assine, M.L., 2014. Ice-keel scour marks in the geologic record: evidence from Carboniferous soft-sediment striated surfaces in the Parana´ Basin, southern Brazil. Journal of Sedimentary Research 84, 26-39.

Weidlich, O., 2002. Middle and Late Permian reefs; distributional patterns and reservoir potential. Special Publication - Society for Sedimentary Geology 72, 339-390.

Wilde, G.L., 2000. Formal Middle Permian (Guadalupian) series; a fusulinacean perspective. Smithsonian Contributions to the Earth Sciences 32, 89-100.

Wilde, G.L., Rudine, S.F., 2000. Late Guadalupian biostratigraphy and fusulinid faunas, Altuda Formation, Brewster County, Texas. Smithsonian Contributions to the Earth Sciences 32, 343-371.

Wilde, G.L., Rudine, S.F., Lambert, L.L., Saller, A.H., Harris, P.M., Kirkland, B.L., Mazzullo, S.J., 1999. Formal designation; Reef Trail Member, Bell Canyon Formation, and its significance for recognition of the Guadalupian-Lopingian boundary. Special Publication - Society for Sedimentary Geology 65, 63-83.

Woodworth-Lynas, C.M.T., Dowdeswell, J.A., 1994. Soft-sediment striated surfaces and massive diamicton facies produced by floating ice, In: Deynoux, M., Miller, J.M.G., Domack, E.W., Eyles, N., Fairchild, I.J., Young, G.M. (Eds.), Earth's Glacial Record. Cambridge University Press, Cambridge, U.K., pp. 241-259.

Young, G.M., 2013. Evolution of Earth's climatic system: Evidence from ice ages, isotopes, and impacts. GSA Today 23, 4-10.

Figure1

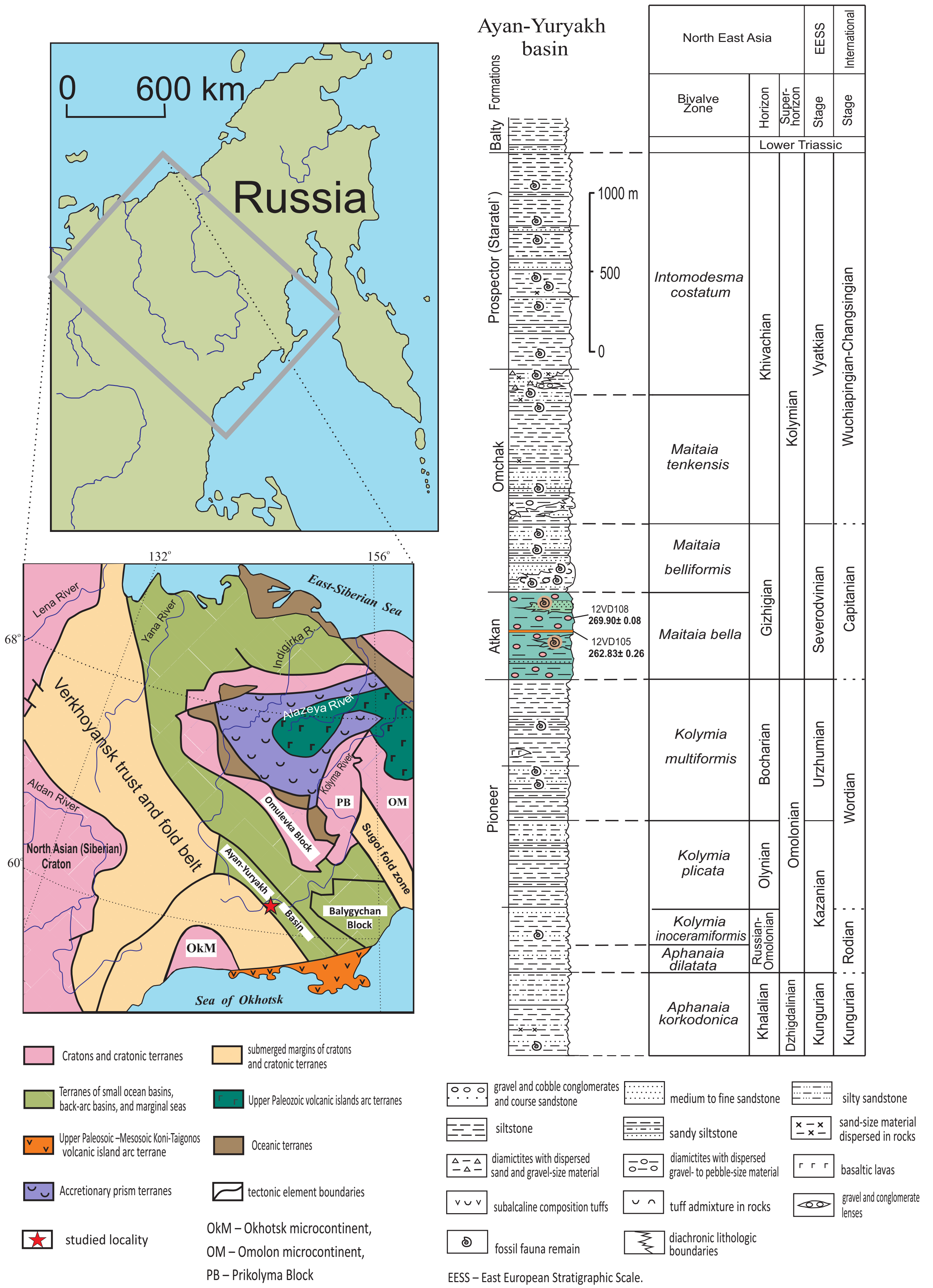

0 600 km
Russia
132°
156°
68°
60°
Lena River
Yana River
Indigirka R.
East-Siberian Sea
Alazeya River
Kolyma River
Verkhoyansk trust and fold belt
Aldan River
North Asian (Siberian) Craton
Omulevka Block
PB
OM
Sugoi fold zone
Ayan-Yuryakh Basin
Balygychan Block
OkM
Sea of Okhotsk
Cratons and cratonic terranes
submerged margins of cratons and cratonic terranes
Terranes of small ocean basins, back-arc basins, and marginal seas
Upper Paleozoic volcanic islands arc terranes
Upper Paleosoic –Mesosoic Koni-Taigonos volcanic island arc terrane
Oceanic terranes
Accretionary prism terranes
tectonic element boundaries
studied locality
OkM – Okhotsk microcontinent,
OM – Omolon microcontinent,
PB – Prikolyma Block
Ayan-Yuryakh basin
Formations
Balty
Prospector (Staratel')
Omchak
Atkan
Pioneer
1000 m
500
0
12VD108
269.90± 0.08
12VD105
262.83± 0.26
North East Asia
EESS
International
Bivalve Zone
Horizon
Super-horizon
Stage
Stage
Lower Triassic
Intomodesma costatum
Maitaia tenkensis
Maitaia belliformis
Maitaia bella
Kolymia multiformis
Kolymia plicata
Kolymia inoceramiformis
Aphanaia dilatata
Aphanaia korkodonica
Khivachian
Gizhigian
Bocharian
Olynian
Russian-Omolonian
Khalalian
Kolymian
Omolonian
Dzhigdalinian
Vyatkian
Severodvinian
Urzhumian
Kazanian
Kungurian
Wuchiapingian-Changsingian
Capitanian
Wordian
Rodian
Kungurian
gravel and cobble conglomerates and course sandstone
medium to fine sandstone
silty sandstone
siltstone
sandy siltstone
sand-size material dispersed in rocks
diamictites with dispersed sand and gravel-size material
diamictites with dispersed gravel- to pebble-size material
basaltic lavas
subalcaline composition tuffs
tuff admixture in rocks
gravel and conglomerate lenses
fossil fauna remain
diachronic lithologic boundaries
EESS – East European Stratigraphic Scale.

Figure2

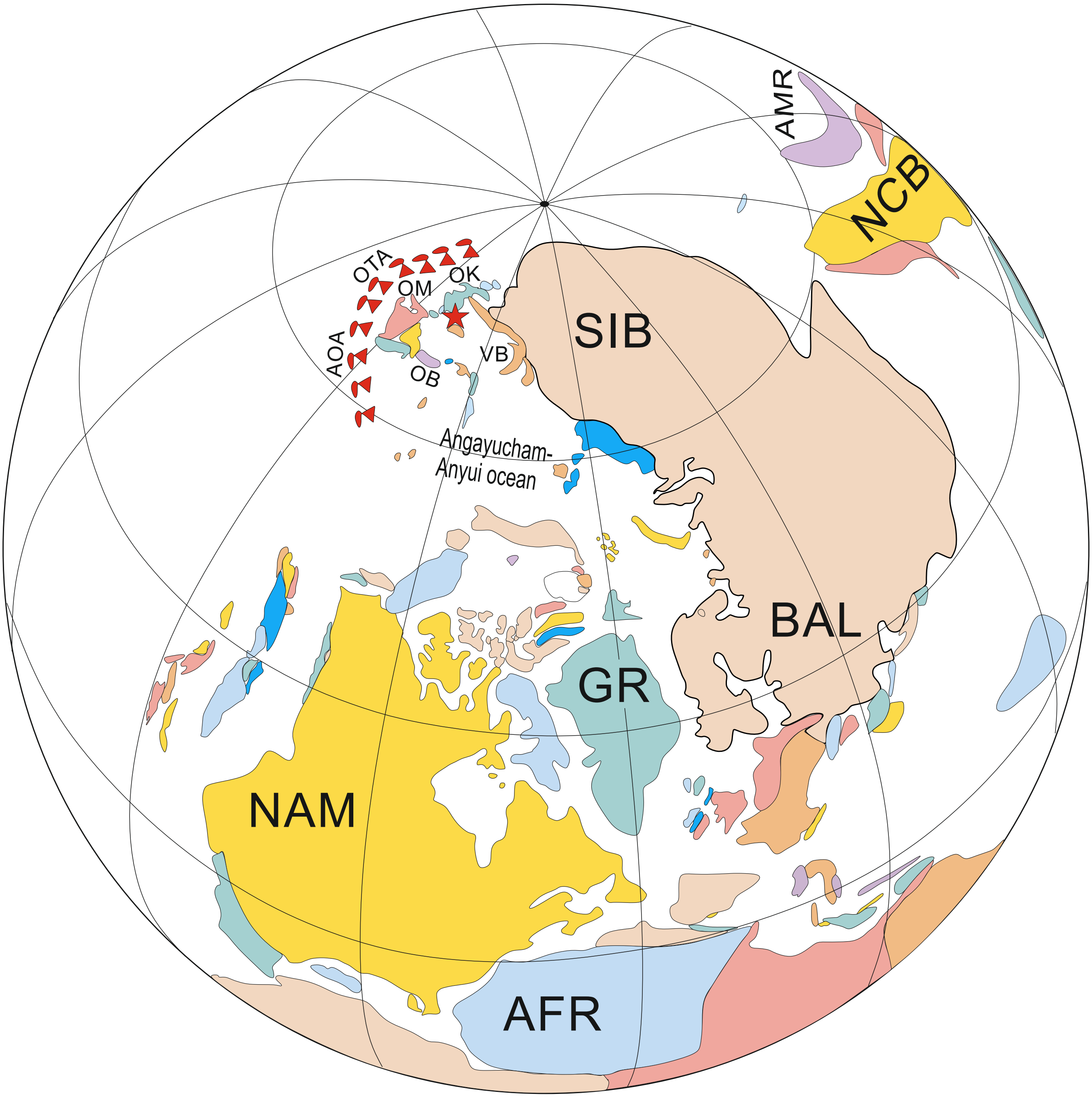

AMR
NCB
OTA
OK
OM
AOA
VB
OB
SIB
Angayucham-
Anyui ocean
BAL
GR
NAM
AFR

Figure3

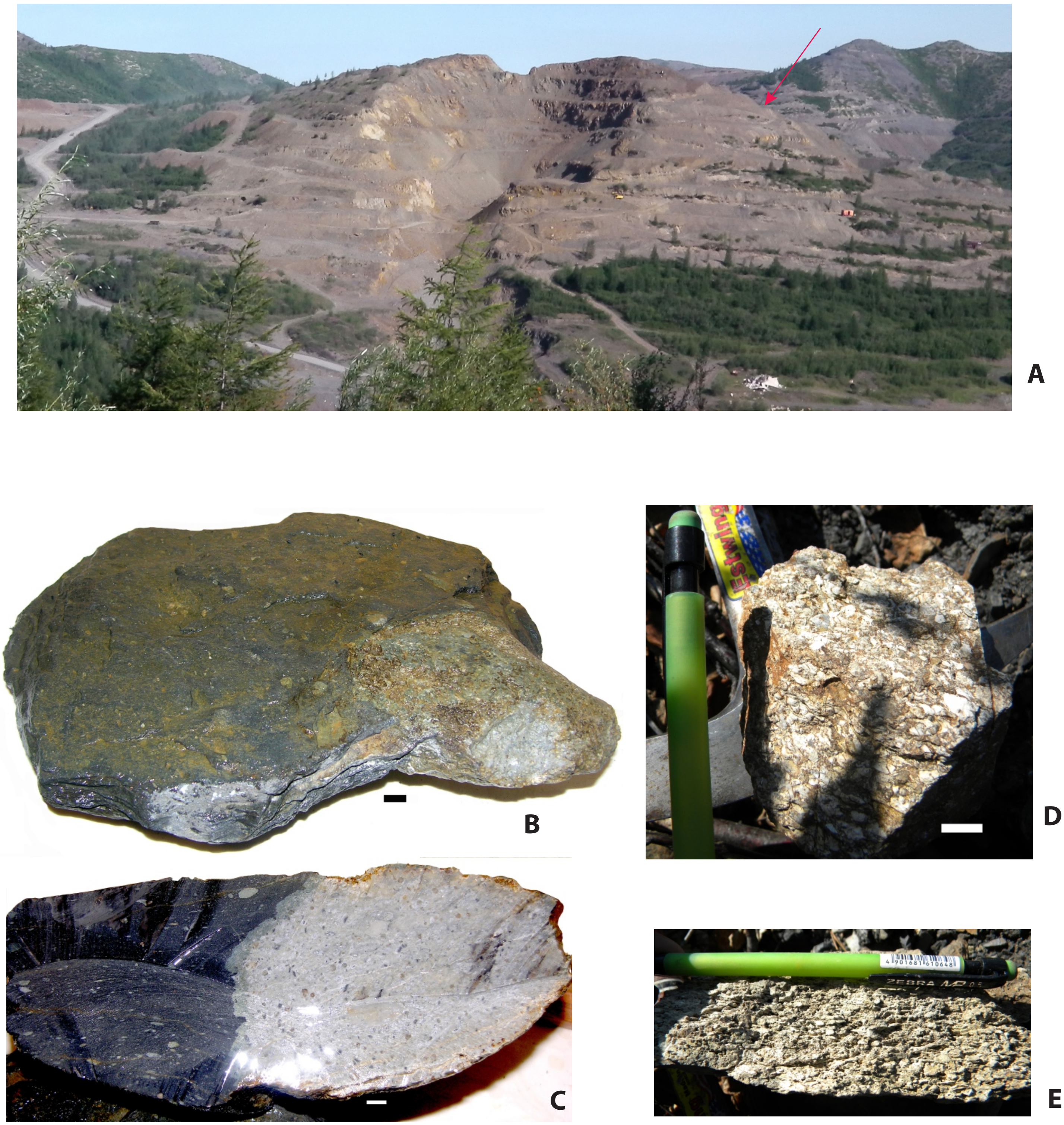

Figure4

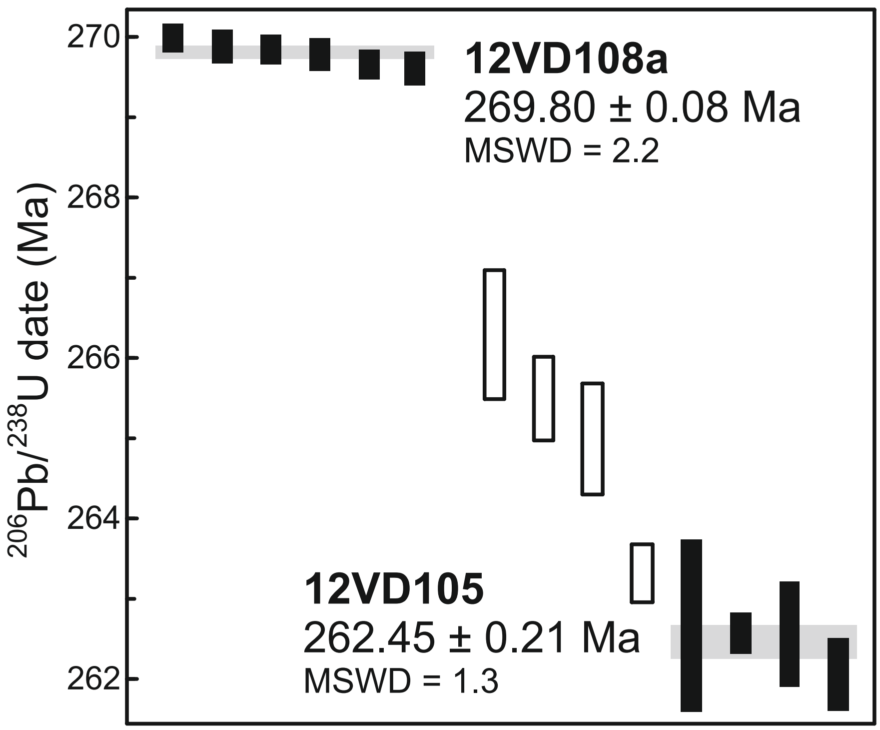
270
268
266
264
262
$^{206}Pb/^{238}U$ date (Ma)
12VD108a
269.80 ± 0.08 Ma
MSWD = 2.2
12VD105
262.45 ± 0.21 Ma
MSWD = 1.3

Figure5

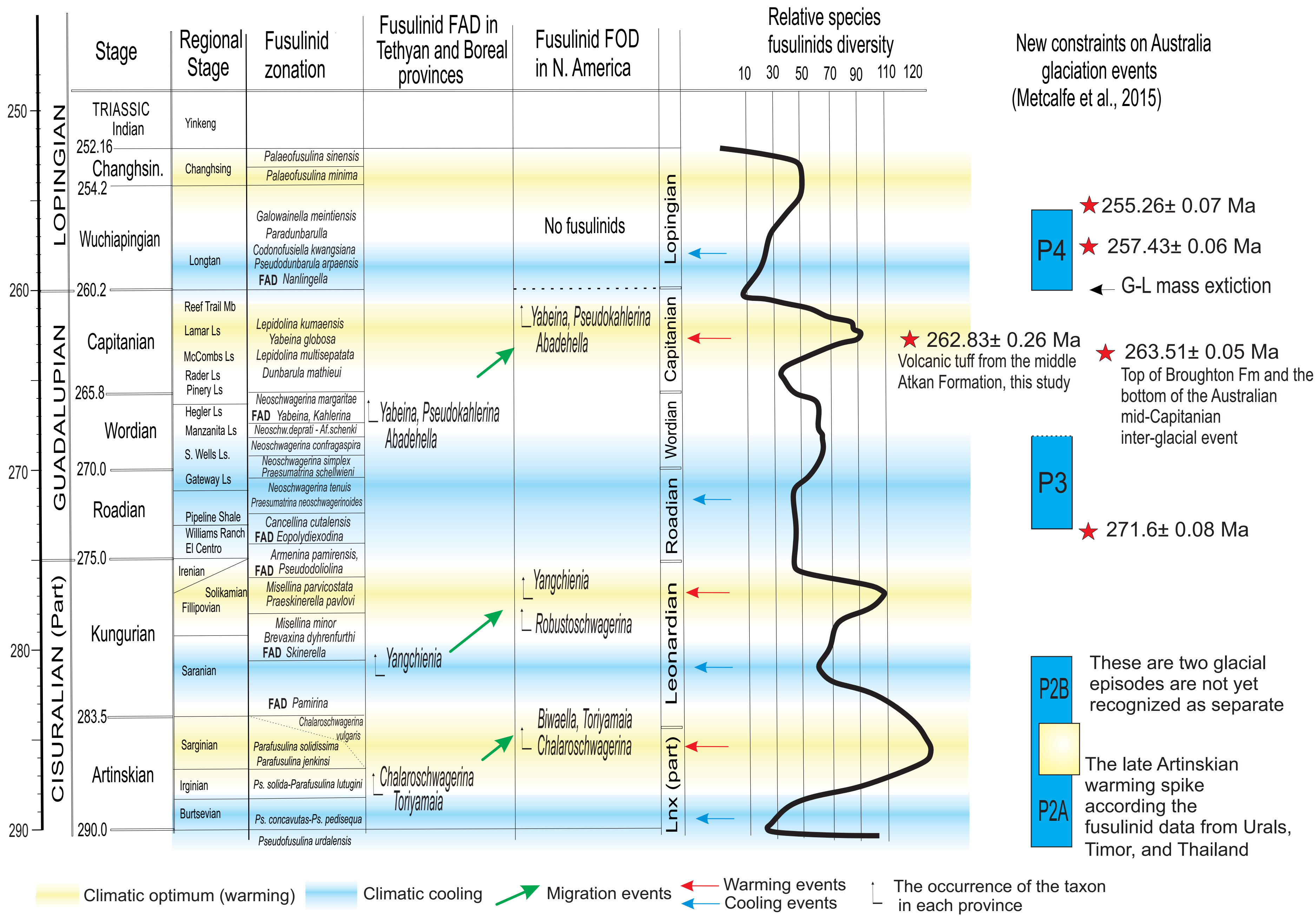

Stage
Regional Stage
Fusulinid zonation
Fusulinid FAD in Tethyan and Boreal provinces
Fusulinid FOD in N. America
Relative species fusulinids diversity
10 30 50 70 90 110 120
New constraints on Australia glaciation events (Metcalfe et al., 2015)
LOPINGIAN
GUADALUPIAN
CISURALIAN (Part)
250
260
270
280
290
TRIASSIC Indian
252.16
Changhsin.
254.2
Wuchiapingian
260.2
Capitanian
265.8
Wordian
270.0
Roadian
275.0
Kungurian
283.5
Artinskian
290.0
Yinkeng
Changhsing
Longtan
Reef Trail Mb
Lamar Ls
McCombs Ls
Rader Ls
Pinery Ls
Hegler Ls
Manzanita Ls
S. Wells Ls.
Gateway Ls
Pipeline Shale
Williams Ranch
El Centro
Irenian
Solikamian
Fillipovian
Saranian
Sarginian
Irginian
Burtsevian
Palaeofusulina sinensis
Palaeofusulina minima
Galowainella meintiensis
Paradunbarulla
Codonofusiella kwangsiana
Pseudodunbarula arpaensis
FAD Nanlingella
Lepidolina kumaensis
Yabeina globosa
Lepidolina multisepatata
Dunbarula mathieui
Neoschwagerina margaritae
FAD Yabeina, Kahlerina
Neoschw.deprati - Af.schenki
Neoschwagerina confragaspira
Neoschwagerina simplex
Praesumatrina schellwieni
Neoschwagerina tenuis
Praesumatrina neoschwagerinoides
Cancellina cutalensis
FAD Eopolydiexodina
Armenina pamirensis,
FAD Pseudodoliolina
Misellina parvicostata
Praeskinerella pavlovi
Misellina minor
Brevaxina dyhrenfurthi
FAD Skinerella
FAD Pamirina
Chalaroschwagerina vulgaris
Parafusulina solidissima
Parafusulina jenkinsi
Ps. solida-Parafusulina lutugini
Ps. concavutas-Ps. pedisequa
Pseudofusulina urdalensis
Yabeina, Pseudokahlerina Abadehella
Yangchienia
Chalaroschwagerina Toriyamaia
No fusulinids
Yabeina, Pseudokahlerina Abadehella
Yangchienia
Robustoschwagerina
Biwaella, Toriyamaia
Chalaroschwagerina
Lopingian
Capitanian
Wordian
Roadian
Leonardian
Lnx (part)
P4
P3
P2B
P2A
★255.26± 0.07 Ma
★ 257.43± 0.06 Ma
G-L mass extiction
★ 262.83± 0.26 Ma
Volcanic tuff from the middle Atkan Formation, this study
★ 263.51± 0.05 Ma
Top of Broughton Fm and the bottom of the Australian mid-Capitanian inter-glacial event
★ 271.6± 0.08 Ma
These are two glacial episodes are not yet recognized as separate
The late Artinskian warming spike according the fusulinid data from Urals, Timor, and Thailand
Climatic optimum (warming)
Climatic cooling
Migration events
Warming events
Cooling events
The occurrence of the taxon in each province

Figure6

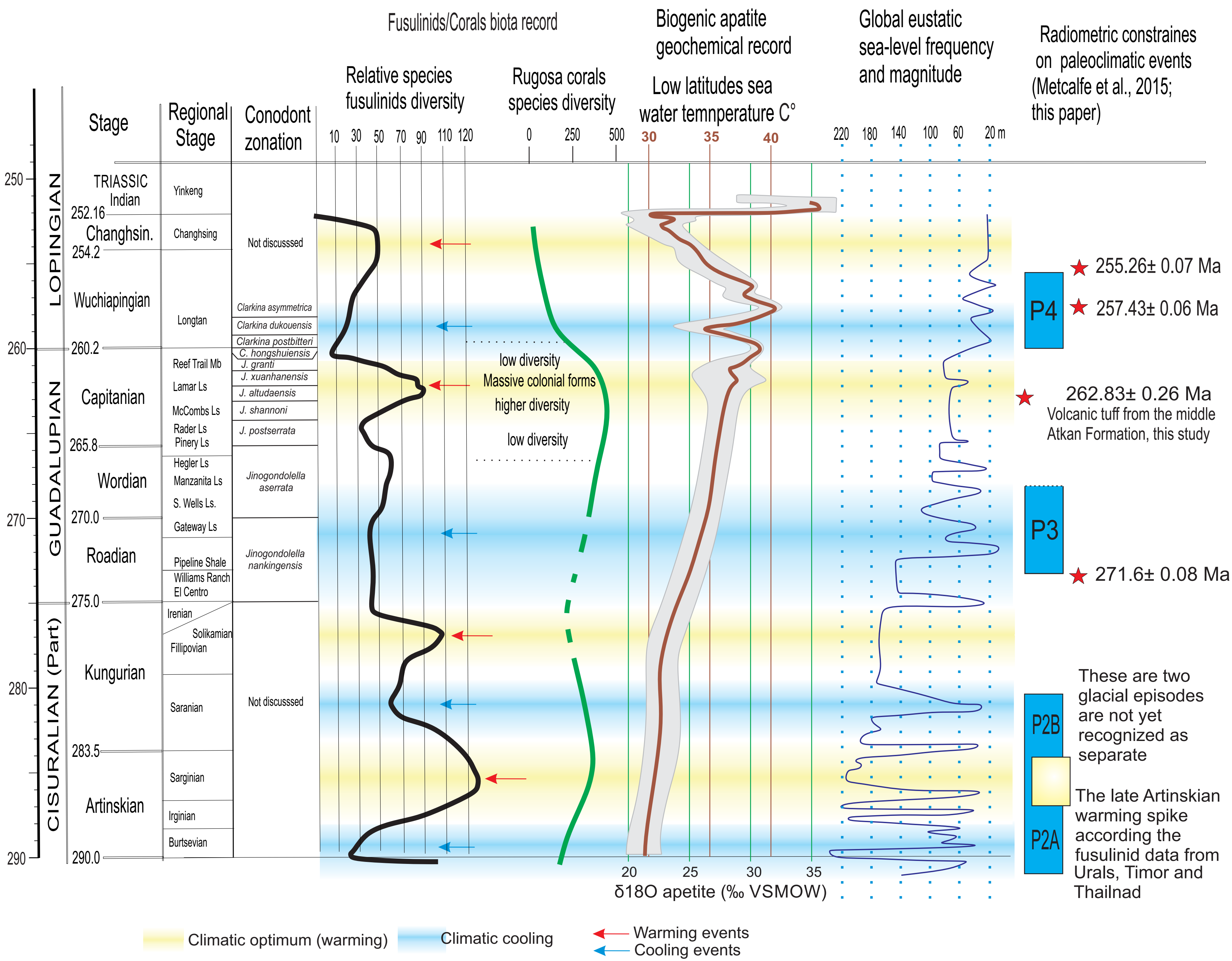

Fusulinids/Corals biota record
Relative species fusulinids diversity
10 30 50 70 90 110 120
Rugosa corals species diversity
0 250 500
Biogenic apatite geochemical record
Low latitudes sea water temnperature C°
30 35 40
Global eustatic sea-level frequency and magnitude
220 180 140 100 60 20 m
Radiometric constraines on paleoclimatic events (Metcalfe et al., 2015; this paper)
Stage
Regional Stage
Conodont zonation
LOPINGIAN
GUADALUPIAN
CISURALIAN (Part)
250
260
270
280
290
TRIASSIC Indian
252.16
Changhsin.
254.2
Wuchiapingian
260.2
Capitanian
265.8
Wordian
270.0
Roadian
275.0
Kungurian
283.5
Artinskian
290.0
Yinkeng
Changhsing
Longtan
Reef Trail Mb
Lamar Ls
McCombs Ls
Rader Ls
Pinery Ls
Hegler Ls
Manzanita Ls
S. Wells Ls.
Gateway Ls
Pipeline Shale
Williams Ranch
El Centro
Irenian
Solikamian
Fillipovian
Saranian
Sarginian
Irginian
Burtsevian
Not discusssed
Clarkina asymmetrica
Clarkina dukouensis
Clarkina postbitteri
C. hongshuiensis
J. granti
J. xuanhanensis
J. altudaensis
J. shannoni
J. postserrata
Jinogondolella aserrata
Jinogondolella nankingensis
Not discusssed
low diversity
Massive colonial forms
higher diversity
low diversity
20 25 30 35
δ18O apatite (‰ VSMOW)
255.26± 0.07 Ma
257.43± 0.06 Ma
P4
262.83± 0.26 Ma
Volcanic tuff from the middle Atkan Formation, this study
P3
271.6± 0.08 Ma
These are two glacial episodes are not yet recognized as separate
P2B
The late Artinskian warming spike according the fusulinid data from Urals, Timor and Thailnad
P2A
Climatic optimum (warming)
Climatic cooling
Warming events
Cooling events

Table1

Table 1. U-Pb isotopic CA-TIMS data.

							Radiogenic Isotope Ratios									
Sample (a)	$\frac{Th}{U}$ (b)	$^{206}Pb^*$ $\times 10^{-13}$ mol (c)	mol % $^{206}Pb^*$ (c)	$\frac{Pb^*}{Pb_c}$ (c)	Pb_c (pg) (c)	$\frac{^{206}Pb}{^{204}Pb}$ (d)	$\frac{^{208}Pb}{^{206}Pb}$ (e)	$\frac{^{207}Pb}{^{206}Pb}$ (e)	% err (f)	$\frac{^{207}Pb}{^{235}U}$ (e)	% err (f)	$\frac{^{206}Pb}{^{238}U}$ (e)	% err (f)	corr. coef.	$\frac{^{207}Pb}{^{206}Pb}$ (g)	± (f)
12VD105																
z1	0.750	0.1322	96.40%	9	0.41	502	0.238	0.051390	0.913	0.293971	0.996	0.041488	0.178	0.536	258.4	21.0
z2	0.726	0.1459	97.23%	11	0.34	652	0.230	0.051499	0.807	0.297964	0.904	0.041963	0.266	0.492	263.2	18.5
z3	0.582	0.3232	98.69%	23	0.36	1375	0.185	0.051630	0.348	0.295922	0.397	0.041570	0.100	0.591	269.0	8.0
z4	0.399	0.5152	98.96%	28	0.45	1729	0.126	0.052048	0.284	0.339725	0.332	0.047340	0.089	0.631	287.5	6.5
z5	0.543	0.1643	97.75%	13	0.31	802	0.172	0.050920	0.588	0.295179	0.666	0.042043	0.201	0.520	237.2	13.6
z6	0.604	0.0604	92.21%	4	0.42	232	0.191	0.049983	2.811	0.290638	2.964	0.042172	0.307	0.536	194.2	65.3
z7	0.683	0.0410	93.71%	5	0.23	287	0.216	0.050825	2.051	0.291297	2.190	0.041568	0.256	0.585	232.9	47.3
z9	0.931	0.0823	96.72%	10	0.23	550	0.295	0.051581	0.908	0.296509	0.980	0.041691	0.140	0.567	266.9	20.8
z10	0.814	0.0326	91.61%	4	0.25	215	0.258	0.049824	3.219	0.285676	3.366	0.041585	0.418	0.406	186.8	74.9
12VD108a																
z1	0.519	1.2358	99.12%	34	0.91	2060	0.164	0.051675	0.200	0.304742	0.245	0.042771	0.068	0.732	271.0	4.6
z2	0.505	0.9075	99.65%	87	0.26	5224	0.160	0.051649	0.120	0.304422	0.170	0.042748	0.070	0.814	269.9	2.7
z3	0.549	0.8097	99.60%	75	0.27	4482	0.174	0.051636	0.143	0.304073	0.193	0.042709	0.078	0.761	269.3	3.3
z4	0.455	0.4759	99.27%	40	0.29	2467	0.144	0.051522	0.226	0.303718	0.272	0.042754	0.082	0.665	264.3	5.2
z5	0.466	0.9950	99.49%	58	0.43	3516	0.148	0.051509	0.167	0.303381	0.210	0.042717	0.071	0.720	263.7	3.8
z6	0.592	0.6129	99.35%	47	0.33	2770	0.187	0.051600	0.199	0.304062	0.245	0.042737	0.077	0.698	267.7	4.6

(a) z1, z2, etc. are labels for analyses composed of single zircon grains or fragments of grains that were annealed and chemically abraded (Mattinson, 2005
Labels in bold denote analyses used in the weighted mean calculations.

(b) Model Th/U ratio calculated from radiogenic 208Pb/206Pb ratio and 207Pb/235U date.

(c) Pb* and Pbc are radiogenic and common Pb, respectively. mol % ^{206}Pb* is with respect to radiogenic and blank Pb.

(d) Measured ratio corrected for spike and fractionation only. Fractionation correction is 0.16 ± 0.06%/amu or 0.18 ± 0.06%/amu (atomic mass unit) (2 si
based on analysis of EARTHTIME 202Pb-205Pb tracer solution.

(e) Corrected for fractionation, spike, common Pb, and initial disequilibrium in 230Th/238U. Common Pb is assigned to procedural blank with compositi
206Pb/204Pb = 18.04 ± 1.22%; 207Pb/204Pb = 15.54 ± 1.04%; 208Pb/204Pb = 37.69 ± 1.26% (2 sigma). 206Pb/238U and 207Pb/206Pb ratios corre
in 230Th/238U using Th/U [magma] = 3.0 ± 0.6 (2 sigma)

(f) Errors are 2 sigma, propagated using algorithms of Schmitz and Schoene (2007) and Crowley et al. (2007).

(g) Calculations based on the decay constants of Jaffey et al. (1971). 206Pb/238U and 207Pb/206Pb dates corrected for initial disequilibrium in 230Th/23
= 3.0 ± 0.6 (2 sigma).